Results

Rvs localization in yeast endocytosis

Averaged centroid tracking, as described in Picco et al., can quantify the movement and dynamics of various endocytic proteins along the timeline of membrane invagination and scission. Briefly described, yeast cells expressing fluorescently-tagged endocytic proteins are imaged at the equatorial plane. Since membrane invagination progresses perpendicularly to the plane of the plasma membrane, proteins that move inward with membrane ingression do so in the imaging plane when imaged in this way. Centroids of many endocytic patches, for example, Sla1-GFP, are thus tracked and averaged, leading to an averaged centroid of high spatial and temporal resolution. When various endocytic proteins are simultaneously imaged with the abundant actin binding protein Abp1, Abp1 provides a frame of reference to which the other proteins can be now aligned.

Centroid tracking shows that the late-stage coat protein Sla1 arrives and accumulates at endocytic sites, starts to moves into the cytoplasm concomitant with the arrival of actin[1,2], for which Abp1 is used as a marker. Sla1 is pulled inwards along with the membrane and follows its movement through endocytosis. It will be used throughout this work as the marker for coat movement. As inward movement of the coat begins, the Sla1 patch is disassembled, inferred from the decay of the fluorescent intensity of Sla1-GFP[2], shown in Fig.2.1. As has been shown before, Rvs localizes to endocytic patches at the yeast plasma membrane in the late scission-stage[1,2]. Rvs167 arrives after a parallel membrane tube is formed, and scission occurs at 60% of its lifetime at the plasma membrane[1,3]. At the time of scission, the Rvs167-GFP centroid shows a sharp jump into the cytoplasm, a profile that is unique among endocytic proteins. Concomitantly, fluorescent intensity of Rvs167-GFP shows a sudden decay. Abp1 intensity also peaks at scission time, and drops, indicating disassembly of the actin network upon vesicle formation.

Dynamics of yeast endocytic proteins

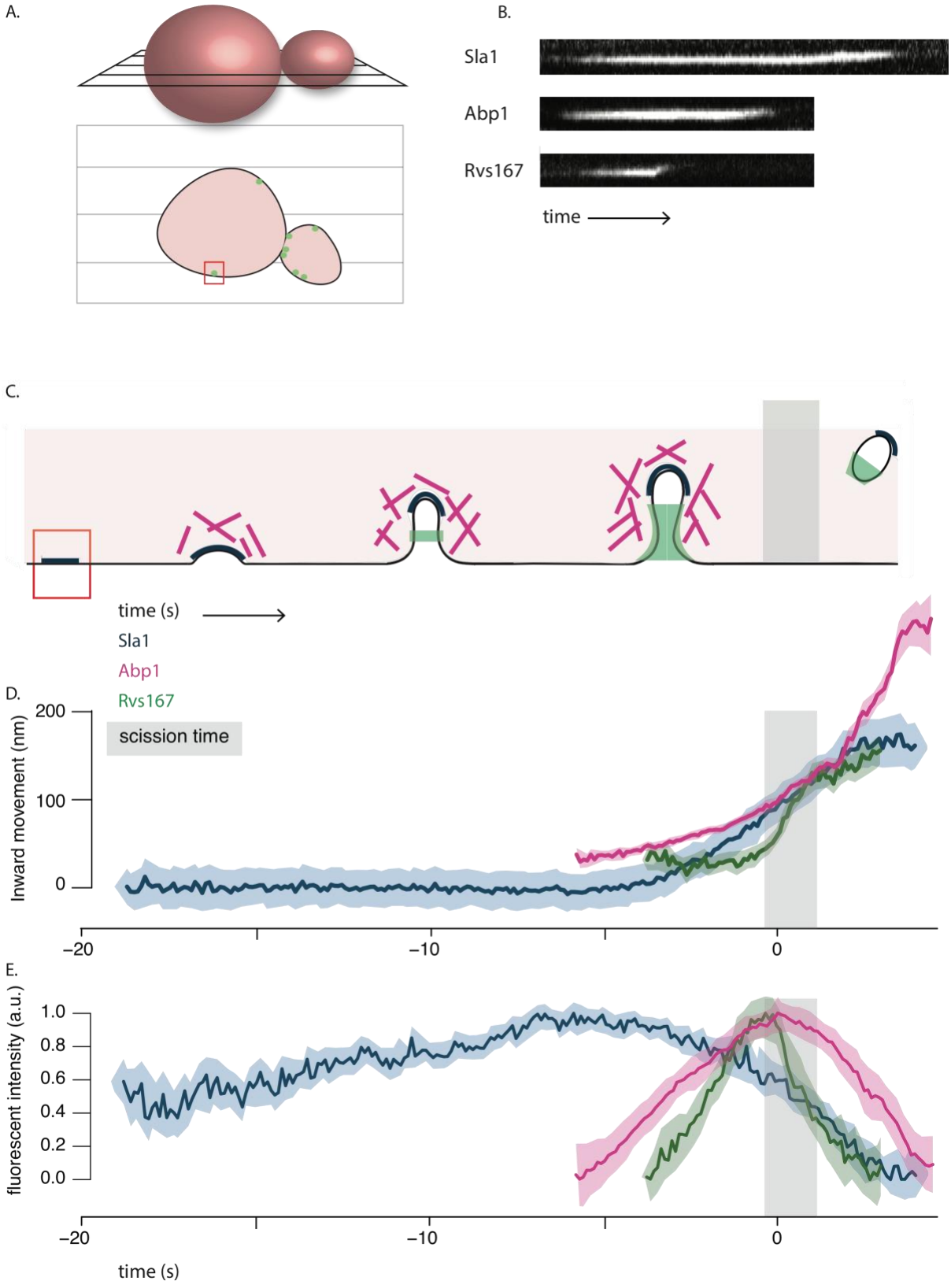

Fig.2.1A: Above: Schematic of a yeast cell, showing the equatorial plane. Below: Cross section of the cell at the equatorial plane, with fluorescently tagged endocytic proteins at the plasma membrane.
B: Kymographs of Sla1-GFP and Rvs167-GFP at endocytic patches at the plasma membrane. Movement of coat protein Sla1-GFP shows slow inward movement, while Rvs167-GFP shows a sharp jump into the cytoplasm that is concomitant with membrane scission and vesicle formation. Exposure rate for kymograph, 80ms, fluorophores excited using 488nm laser.
C: Schematic of the timeline of membrane invagination during endocytosis, with Sla1, Abp1 and Rvs167 indicated.
D, E: Movement and normalized fluorescent intensity of averaged centroids of Sla1, Abp1 and Rvs167 across the endocytic timeline. Sla1 follows the membrane as it is pulled inwards into the cytoplasm. Rvs arrives at membrane tubes, potentially forming a scaffold around the tube. Upon membrane scission, the scaffold along the tube is disassembled, resulting in an inward jump of the Rvs167 centroid (to protein localized at the base of the newly formed vesicle), and a sharp decay in its fluorescent intensity. Abp1 intensity also drops after membrane scission. D and E are aligned in time so that time=0 (sec) corresponds to the maximum of fluorescent intensity of averaged Abp1 patches.

R0. Deletion of Rvs167 leads to shorter invaginations

The Rvs complex, as has been discussed in section {Intro}, has been identified as having an influence on membrane scission efficiency. Recruitment in the final stage of membrane ingression, localization to the membrane tube, and concomitant disassembly with scission all indicate that Rvs could mechanistically influence the scission process. In order to quantify this influence, I tracked Sla1-GFP in rvs167del cells and comparted averaged centroid movement against WT Sla1-GFP movement. Movement of Sla1 is reduced in rvs167 deletion, to about 60nm instead of 140nm in WT cells. CLEM studies have shown that Rvs167 localizes to endocytic sites after the tubes are 60nm long: membrane invagination is unaffected till the expected time of arrival of Rvs, after which membrane scission occurs, rather than further invagination. This indicates that first, membrane scission can occur at invagination lengths of 60nm. Then, that the arrival of Rvs prevents membrane scission at this point and allows further membrane invagination.

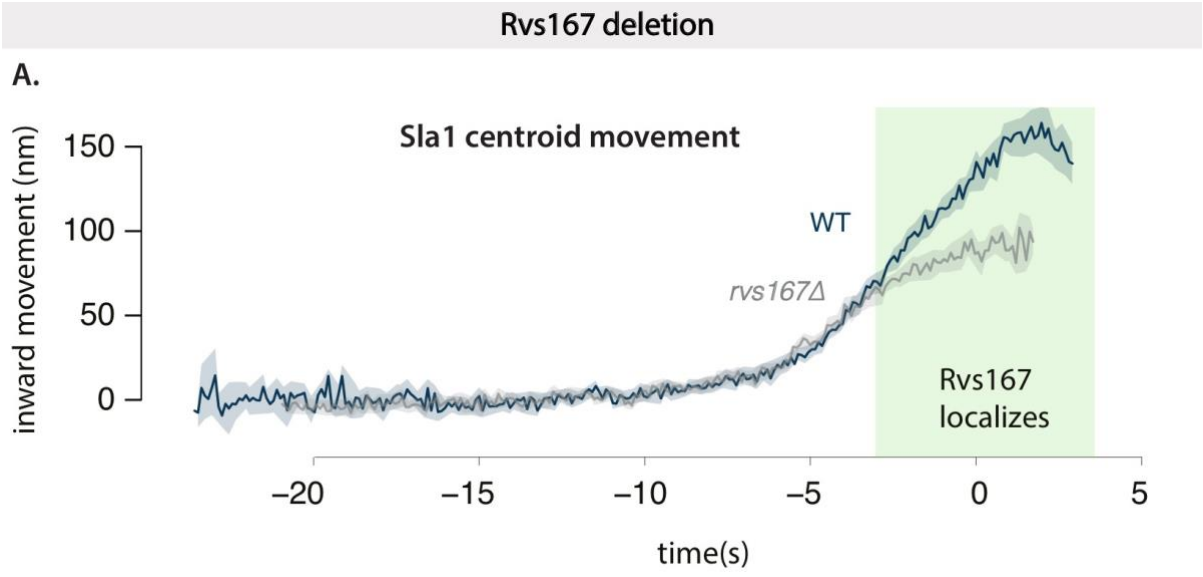

Fig.2.2: Averaged centroid movement of Sla1-GFP in WT and rvs167del cells. About 40 endocytic patches from 10-15 yeast cells are included in the averages. WT Sla1 is aligned in time so that time=0 (sec) corresponds to

scission time, determined by the maxima of fluorescent intensity of Abp1. Averaged centroid of Sla1-GFP in rvs167del cells is shifted in time so that inward movement is concomitant with WT Sla1 movement.

R1. Recruitment of Rvs and function of domains:

Curvature-generation vs sensing function of BAR proteins:

Cellular membrane shape is a result of properties like rigidity, tension, intracellular pressure, that are all influenced by membrane lipid composition and the proteins embedded in it[4,5]. Since tension, pressure, and rigidity all oppose membrane deformation, energy is required to deform and bend it. BAR domains can generate curvature if the energy required to deform the membrane is less than the energy spent in binding flat membrane.

Curvature-generation by scaffolding and imposing its own shape on membranes has been extended to various types of BAR proteins, (Arkhipov et al., 2009; Frost et al., 2008; Henne et al., 2007; Itoh et al., 2005; Pykalainen et al., 2011; Saarikangas et al., 2009; Shimada et al., 2007; Yu and Schulten, 2013). In order for BAR scaffolds to impose membrane curvature, some requirement have to be met[6]: they have to have present a large membrane-interacting surface that can mediate membrane binding, have intrinsic curvature that can be imposed on the surface, and have a rigid structure that can overcome bending resistance of the membrane. Because of their shape (Peter 2004, Gallop 2006, Weissenhorn 2005), and their capacity to oligomerize into large assemblies on tubes (Mim 2012, Mizuno 2010, Takei 1999, Yin 2009), it has been suggested that BAR domains impose their shape on the membrane, and generate membrane curvature on cellular membranes. Further, it has been shown that the central BAR region is rigid and required for tubulation, both *in-vivo* and of liposomes[7]. The N-helix of NBAR domains can also generate curvature independently of the BAR scaffold (Varkey 2010, Westphal and Chandra 2013). In endophilin, the BAR domain is relatively far from the membrane, suggesting a mechanism dependent on the N-helix (Jao 2010). Different BAR domains thus likely employ different mechanisms to interact with the membrane for generating vesicles, and tubes (Ambroso 2014). For example, the N-helix of endophilin is necessary for liposome binding[8], while that of amphiphysin is important, but not necessary[9].

Curved BAR proteins that can induce curvature are also able to sense curvature: in-vitro, BAR domains show a preferential-binding to vesicles based on their intrinsic curvature. Curvature-generation and sensing seem to intrinsically coupled mechanisms. That BAR domains are able to generate curvature does not imply that this is their function, at least in endocytosis: *in-vivo*, the significance of curvature-generation is not determined. Tracking over thirty different endocytic proteins in NIH-3TC cells (derived from mouse fibroblasts), TIRF imaging shows that Endophilin2 and Amphiphysin1 arrive late in the endocytic time-line right before scission[10], suggesting they arrive when membrane tubes are already formed.

In the case of Rvs, centroid tracking and averaging shows that the complex localizes to sites late in the endocytic timeline, close to scission[2]. CLEM studies have further shown that Rvs localizes to sites after the membrane invaginations are about 60nm deep into the cytoplasm: Rvs localizes once membrane curvature is established. Whether this localization is dependent on membrane curvature, recognized by the BAR domain has not been shown.

R1.1 BAR domains sense membrane curvature in-vivo

To test whether Rvs is recruited because of membrane curvature, I first imaged Rvs167-GFP without the BAR domain, that is Rvs167-delsh3-GFP (henceforth BAR-GFP). BAR-GFP forms cortical patches (Fig.2.2A), so BAR domain is able to localize to the plasma membrane in the absence of the SH3 domain. In a yeast strain expressing both BAR-GFP and Abp1-mCherry, BAR-GFP co-localizes with Abp1, indicating that BAR domains are recruited to endocytic patches (Fig2.2A, C). In order to test whether this localization is due of membrane curvature, I compared the dynamics of Rvs167-GFP against BAR-GFP in sla2del cells (Fig2.2D-F). Sla2 is a coat protein that acts as a linker between the membrane and the actin cytoskeleton by binding both via its N-terminal ANTH domain, and its C-terminal THATCH domain. This allows forces generated within the actin network to be transmitted to the membrane[11]. In sla2del cells, rather than cortical actin patches, an "uncoupling phenotype" is observed[11,12]. Although endocytic coats are formed, actin is polymerized continuously at these sites, the membrane is not pulled inwards, and vesicles are not formed: forces generated by the actin network are not transmitted to the membrane (Fig.2.2E).

In sla2del cells, Rvs167-GFP is recruited to the plasma membrane (Fig.2.2D,F) at the plasma membrane, and together with Abp1-mCherry. Some Rvs167-GFP patches persist at the plasma membrane, while many are assembled and disassembled at Abp1 patches. Some Rvs167 patches do not co-localize with Abp1. In sla2del cells expressing BAR-GFP, localization is mostly removed except for rare transient patches at the plasma membrane that are co-localized with Abp1, while most of the patches appear to be recruited independent of Abp1. Rvs167-GFP and BAR-GFP patches are both dynamic, indicating an interaction exists in both cases that is able to assemble and disassemble Rvs patches at the plasma membrane.

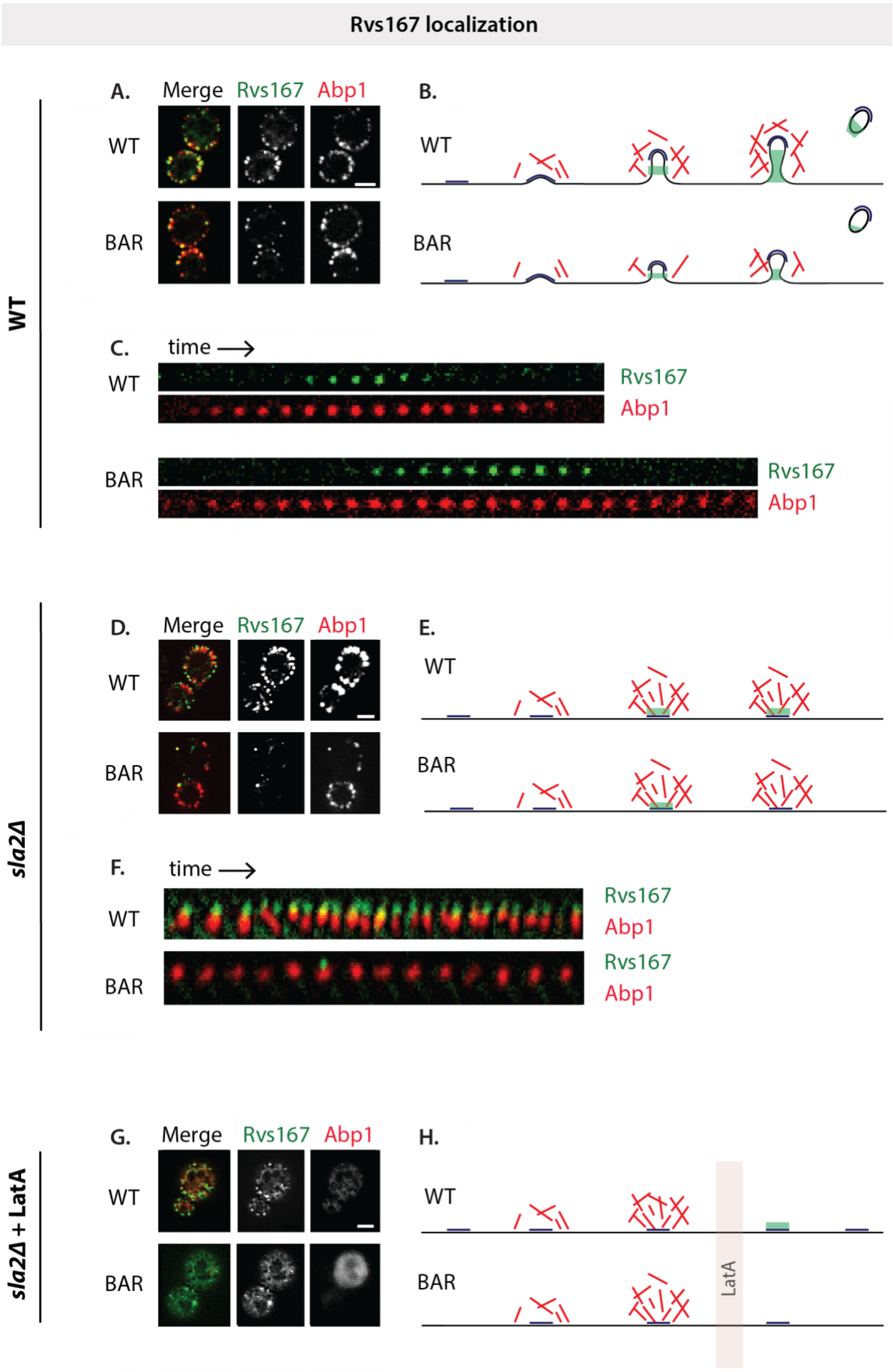
Rvs167 localization
WT
A.
Merge
Rvs167
Abp1
WT
BAR
B.
WT
BAR
C.
time
WT
Rvs167
Abp1
BAR
Rvs167
Abp1
sla2Δ
D.
Merge
Rvs167
Abp1
WT
BAR
E.
WT
BAR
F.
time
WT
Rvs167
Abp1
BAR
Rvs167
Abp1
sla2Δ + LatA
G.
Merge
Rvs167
Abp1
WT
BAR
H.
WT
BAR
LatA

Fig.2.2: **A**: Maximum intensity projections of time-lapse images of cells expressing either Rvs167-GFP and BAR-GFP along with Abp1-mCherry. Exposure rate 250ms, GFP and RFP channels excited using 488 and 561nm lasers respectively. **B**: Schematic of membrane progression of in WT and BAR endocytic events (BAR invaginations are shorter, and recruit fewer Rvs molecules: see section R1.3).
C: Montage of Rvs167-GFP and BAR-GFP localizations on the plasma membrane with Abp1-mCherry. Each frame of montage is every third frame of time-lapse images.
D: Maximum intensity projection of time-lapse images of sla2del cells expressing either full-length Rvs167-GFP or BAR-GFP with Abp1-mCherry.
E: Schematic of membrane invagination in the absence of Sla2, in which membrane is decoupled from forces generated by actin polymerization. **F**: Montage of Rvs167-GFP BAR-GFP with Abp1-mCherry. Exposure rate 1000ms for GFP, 800ms for RFP, excited using 488 and 561nm lasers.
G: Maximum intensity projection of time-lapse images of sla2del cells expressing either full-length Rvs167-GFP or BAR-GFP, along with Abp1-mCherry, after treatment with LatA for 10'. Exposure rate 1000ms for GFP, 800ms for RFP. **H**: Schematic of membrane invagination in Sla2del cells treated with LatA.
All scale bars = 2um.

R1.2 The SH3 domain is able to localize Rvs in an actin and curvature-independent manner

As I show in the previous section, full-length Rvs is able to localize to cortical patches in Sla2del cells. This localization must come from the SH3 domain, since BAR alone does not localize in cells without sla2. We expected that the SH3 domain must interact with WASP or actin-binding proteins: an interaction with Abp1 has been shown, as well as with Las17, type I Myosins, and Vrp1. In order to prove this, I imaged BAR-GFP and Abp1-mCherry in sla2del cells treated with the actin sequestering agent LatrunculinA (LatA). LatA is a sea-sponge toxin that binds monomeric actin and prevents incorporation of actin into filaments. Since high actin turnover is required at endocytic sites, LatA effectively disassembles WASP components and other actin-binding proteins of the endocytic machinery, and blocks endocytosis. In combination with the sla2 deletion, latA treatment will effectively prevent membrane curvature as well as remove actin-binding proteins from endocytic sites. Loss of actin binding proteins is verified by the loss of Abp1 signal in the RFP channel.

Surprisingly, full-length Rvs is transiently localized to the plasma membrane in spite of the LatA treatment, suggesting that the SH3 domain is able to recruit Rvs to the plasma membrane. This recruitment occurs in the absence of a BAR-membrane interaction, since BAR-GFP localization is completely removed in LatA treated cells. Rvs167-GFP patches are transient, so an assembly-disassembly mechanism is mediated by the SH3 domain outside of its BAR domain interaction. Localization of Rvs161, which does not have an SH3 domain, is also removed by LatA treatment[12], supporting the conclusion that the BAR domains of the Rvs complex senses membrane curvature in-vivo.

R1.3 Loss of the SH3 domain affects endocytic progression

Since the SH3 domain plays a surprisingly larger role in the function of Rvs, I investigated its effect further. The SH3 domain generally mediates protein-protein interaction by binding to proline-rich sequences that contain a core PXXP motif[13,14] (where X is any amino acid). These domains are ubiquitous in cellular interaction pathways, and several endocytic proteins have at least one SH3 domains, used to self-regulate activity, as well as to modulate local concentrations of protein. Although SH3 domains are abundant, they appear to have specific of binding partners. For Rvs167 SH3, neither the specific binding partner, nor its function in the scheme of endocytosis is known. From early work, the BAR domain is expected to act as

the functional module of the Rvs proteins: most phenotypes of Rvs deletion can be compensated by expression of the BAR domain alone, although the SH3 domain is required in addition to the BAR domain for bipolar budding pattern[15].

In order to probe the contribution of the Rvs SH3 domain to endocytosis, I studied coat and Rvs dynamics by expressing Rvs167 without the SH3 domain. Quantification of the number of BAR-GFP molecules[2] recruited to endocytic sites shows that without the SH3 domain, recruitment is reduced by nearly half (30.1 +/- 9.9 for BAR-GFP compared to 53.2 +/- 5.3 for Rvs167-GFP), although the cytoplasmic concentration of protein is not affected compared to Rvs167-GFP. The inward jump of BAR-GFP is reduced, compared to the full-length protein, and a number of BAR-GFP patches remain on the plasma membrane and are disassembled without inward movement. Movement of the coat protein Sla1 is similarly reduced. Sla1 moves in to approximately 50nm instead of the 140nm found in WT invaginations. Abp1-GFP recruitment without the SH3 domain is reduced to 50% of WT recruitment, from 347+/- 30.6 molecules in WT to 172.6 +/- 12.9. Shorter invaginations with a maximum of 60nm have been observed in the case of Rvs167 deletion by CLEM [3], which is about the same length as those observed in the SH3 deletion: loss of the SH3 domain appears to be detrimental to the function of the Rvs complex.

For a more detailed inquiry into changes in the endocytic machinery without the Rvs167 SH3 domain, I quantified the lifetimes of Rvs, and coat and actin network using Sla1 and Abp1 as markers in SH3 deleted cells using total internal reflection fluorescence (TIRF) microscopy. Unlike epifluorescence microscopy at the equatorial plane, that has been the method used for quantification so far, when using TIRF, only fluorophores up to a depth of about 100nm from the glass-sample interphase are excited. This reduces fluorescent signal from the cytoplasm, allowing detection of low intensity fluorescent signal, and is a better method for quantification of protein lifetime than epifluorescence microscopy. Although this method is sensitive to low fluorescent intensity, once the proteins start to move inwards inot the cytoplasm, fluorescent intensity rapidly drops, since only ~100nm from the glass-sample interphase is excited. Therefore, rather than a quantification of the entire lifetime of the protein, this is a quantification of the non-motile lifetime of a protein that arrives at endocytic sites, and moves along with the plasma membrane, or at scission, like Sla1 and Rvs167. Non-motile lifetimes of BAR-GFP, Sla1-mCherry and Abp1-mCherry in SH3 deleted cells is thus compared against WT Rvs167-GFP, Sla1-mCherry and Abp1-mCherry.

While lifetimes of Rvs167 and BAR measured in this way are similar, and Sla1 lifetime with and without the SH3 domain is also similar, there is a significant increase in the lifetime of Abp1 lifetime in the absence of the SH3 domain. I then looked for differences in the sequence of recruitment of these endocytic proteins by looking at the difference in time between recruitment of Sla1 and Rvs, and the difference in time between recruitment of Abp1 and Rvs in the WT and SH3 deleted strain. The time difference between recruitment of Sla1 and full-length and SH3 deleted Rvs167 is unchanged, while the difference in time between recruitment of Abp1 and BAR is increased when compared to WT Rvs.

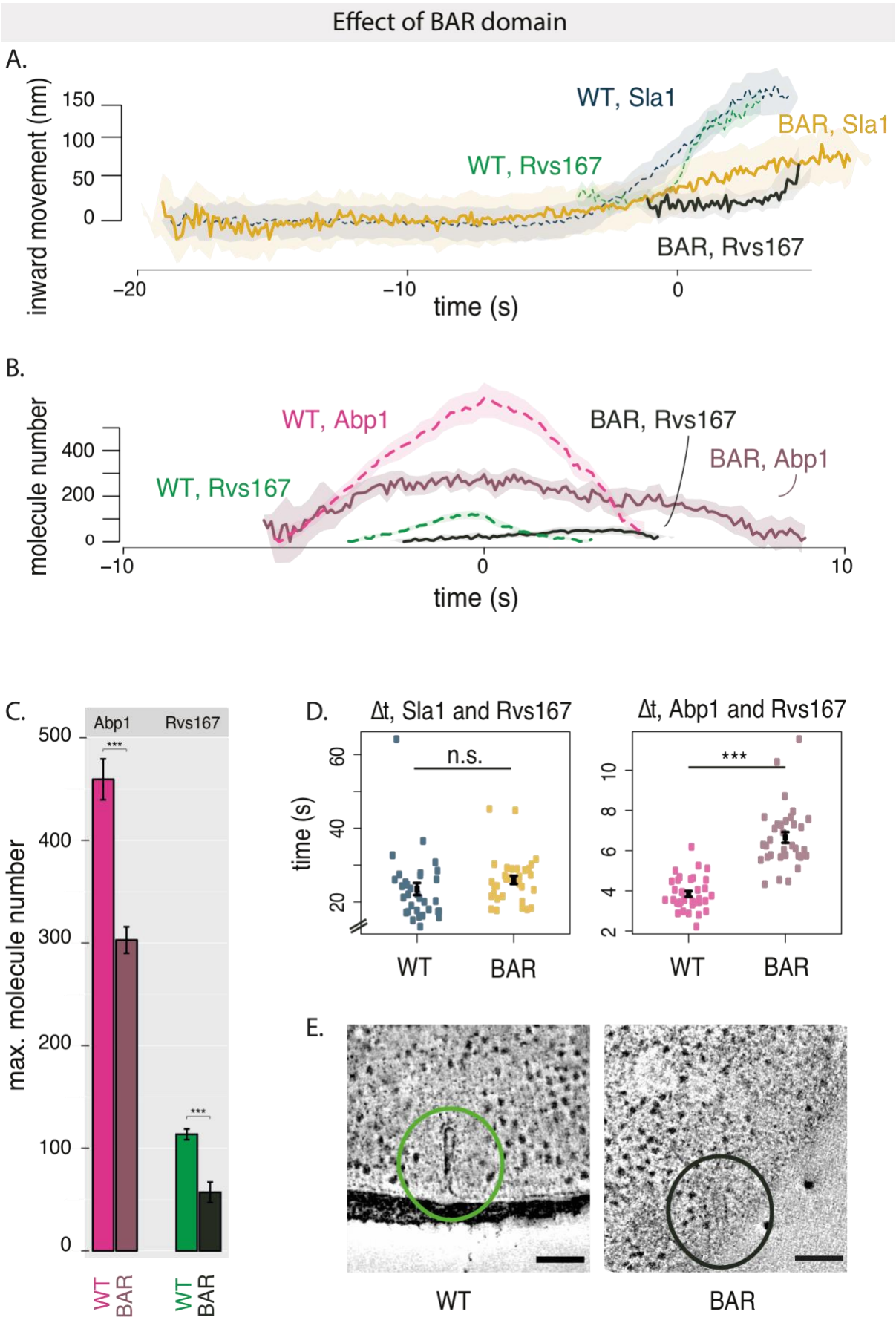
Effect of BAR domain
A.
inward movement (nm)
150
100
50
0
WT, Sla1
BAR, Sla1
WT, Rvs167
BAR, Rvs167
−20
−10
0
time (s)
B.
molecule number
400
200
0
WT, Abp1
BAR, Rvs167
BAR, Abp1
WT, Rvs167
−10
0
10
time (s)
C.
Abp1
Rvs167
max. molecule number
500
400
300
200
100
0
***
***
WT
BAR
WT
BAR
D.
Δt, Sla1 and Rvs167
Δt, Abp1 and Rvs167
time (s)
60
40
20
n.s.
***
10
8
6
4
2
WT
BAR
WT
BAR
E.
WT
BAR

Fig.2.3 A: Averaged centroid movement of Sla1 and Rvs167 in WT and BAR strains. Centroids are aligned in time so that time=0 corresponds to the Abp1-mCherry fluorescent intensity peak in simultaneous dual-color imaging of the corresponding strains.
B: Molecule numbers of Abp1-GFP and Rvs167-GFP and BAR-GFP with standard error of mean.
C: Lifetimes are measured by TIRF in Rvs167-GFP/ Abp1-mCherry and Rvs167-GFP/ Sla1-mCherry strains in WT and BAR strains. Exposure 560ms for each channel. Mean and standard error of the mean are shown, * = p≤0.05, ** = p≤0.01, *** = p≤0.001. P values of two-sided t test.
D: Difference in time between arrival of Sla1-mCherry and Rvs167-GFP, and Abp1-mCherry and Rvs167-GFP in WT and BAR strains. Exposure 560ms for each channel. Mean and standard error of the mean are shown, * = p≤0.05, ** = p≤0.01, *** = p≤0.001. P values of two-sided t test.

Fig.2.4 A: Distribution of invagination lengths obtained using CLEM. Rvs167-GFP and Abp1-mCherry are tagged in WT and BAR strains. Invaginations similar to WT are seen in BAR strain, although distribution shows shorter invaginations, similar to centroid tracking data.

Scission mechanisms:

Several membrane scission mechanisms for yeast endocytosis have been proposed in the last years, in the absence of conclusive mechanistic evidence. Since we know that Rvs plays a major and unique role in determining the efficiency of membrane scission, I have focused of models that assign a central role to BAR domain proteins In the following pages, I discuss their propositions, describe experiments that have tested these mechanisms, and the conclusions they propose.

Does yeast dynamin Vps1 influence membrane scission?

Yeast dynamin is the obvious solution to membrane scission. Although none of the three dynamin-like yeast proteins has a proline-rich domain, one of the yeast dynamins, Vps1 has been suggested to be involved in endocytosis[16,17]. Rooij et al., suggest that Vps1 localizes to endocytic sites in the late scission stage, and that the *vps1*Δ *rvs167*Δ double mutant increases membrane retraction rates after invagination, an indication of scission failure. Vps1-GFP does not localize to endocytic sites in Gadila et at.,[18], but localizes to the golgi body and to vacuoles. Kishimoto et al, do not find a colocalization between Vps1 and Abp1 localization, and also report that the *vps1*Δ *rvs167*Δ double mutation does not affect membrane retraction rates. Vps1 tagged with both GFP as well as superfolded GFP, and imaged by TIRF microscopy fails to colocalize with Abp1 (data not shown, personal communication with Andrea Picco). The debate concerning the involvement of Vps1 in membrane scission in yeast has been compounded by the possibility that the GFP tag at the Vps1 C-terminal could interfere with its localization to endocytic sites, and/or its interaction with the Rvs complex.

R2.1 Vps1 does not affects coat or scission protein dynamics

I investigated the role of Vps1 by studying coat and scission proteins in *vps1*Δ cells. The late coat protein, Sla1 is used as a marker for coat movement, and Rvs167 is used as the scission marker. Centroid tracking and averaging is performed as described in Picco et al., and inward movements of both in wild-type and *vps1*Δ cells are compared.

*vps1*Δ cells exhibit a growth defect at 37C, as has been reported[16]. *vps1*Δ cells expressing Sla1-GFP, are imaged using epifluorescence microscopy. Sla1 accumulates in patches at the plasma membrane, moves inwards, and disassembles like in WT. Sla1-GFP centroids from multiple cells are tracked and averaged. The centroid movements and intensities are plotted in time and space in Figure3C and 3D. WT Sla1-GFP centroid movement in 3C is aligned in

time so that time=0 corresponds to the maximum of the averaged Abp1-mCherry fluorescent intensity acquired from simultaneous two-channel images of Sla1-GFP and Abp1-mCherry in WT cells, as described in Picco et al. The maximum of the Abp1 fluorescent intensity in WT corresponds to scission time. At scission time, the Sla1 at endocytic patches is quickly disassembled, as seen in the fluorescent intensity decay in 3D. Averaged centroid dynamics of Sla1-GFP of the *vps1*Δ strain is acquired from single channel imaging of Sla1-GFP, and this is shifted arbitrarily in time compared to the WT for visualization purposes. The fluorescent intensity trace of Sla1-GFP in *vps1*Δ in 3D is shifted in time to that the maxima is aligned to the WT Sla-GFP maxima, in order to easily compare rate of assembly and disassembly of the patches. The lifetime of Sla1-GFP appears to be slightly shortened in *vps1*Δ compared to the WT, but this shortening occurs early in the lifetime of the protein at endocytic patches, when the molecule numbers of Sla1 are low, and epifluorescent microscopy is not particularly sensitive in this range of fluorescent intensity. Therefore, I do not take this to indicate a true shortened lifetime; lifetime of Sla1-GFP in *vps1*Δ were not investigated further. In WT cells, Sla1 moves into the cytoplasm about 140nm before membrane scission occurs. If Vps1 was required for membrane scission, Sla1 would be expected to undergo delayed or failed scission. However, *vps1*Δ does not increase the rate of membrane retraction. Inward movement of Sla1 is also not changed: it moves inward at the same rate, and to similar maxima of 140nm.

The averaged centroid of Rvs167 would not show the sharp jump into the cytoplasm if scission failed in *vps1*Δ. The inward movement of Rvs167, however, remains the same as in WT. I conclude that if Vps1 does localize to endocytic patches in *S.cerevisiae*, it is not involved in regulating membrane scission.

Dynamin deletion

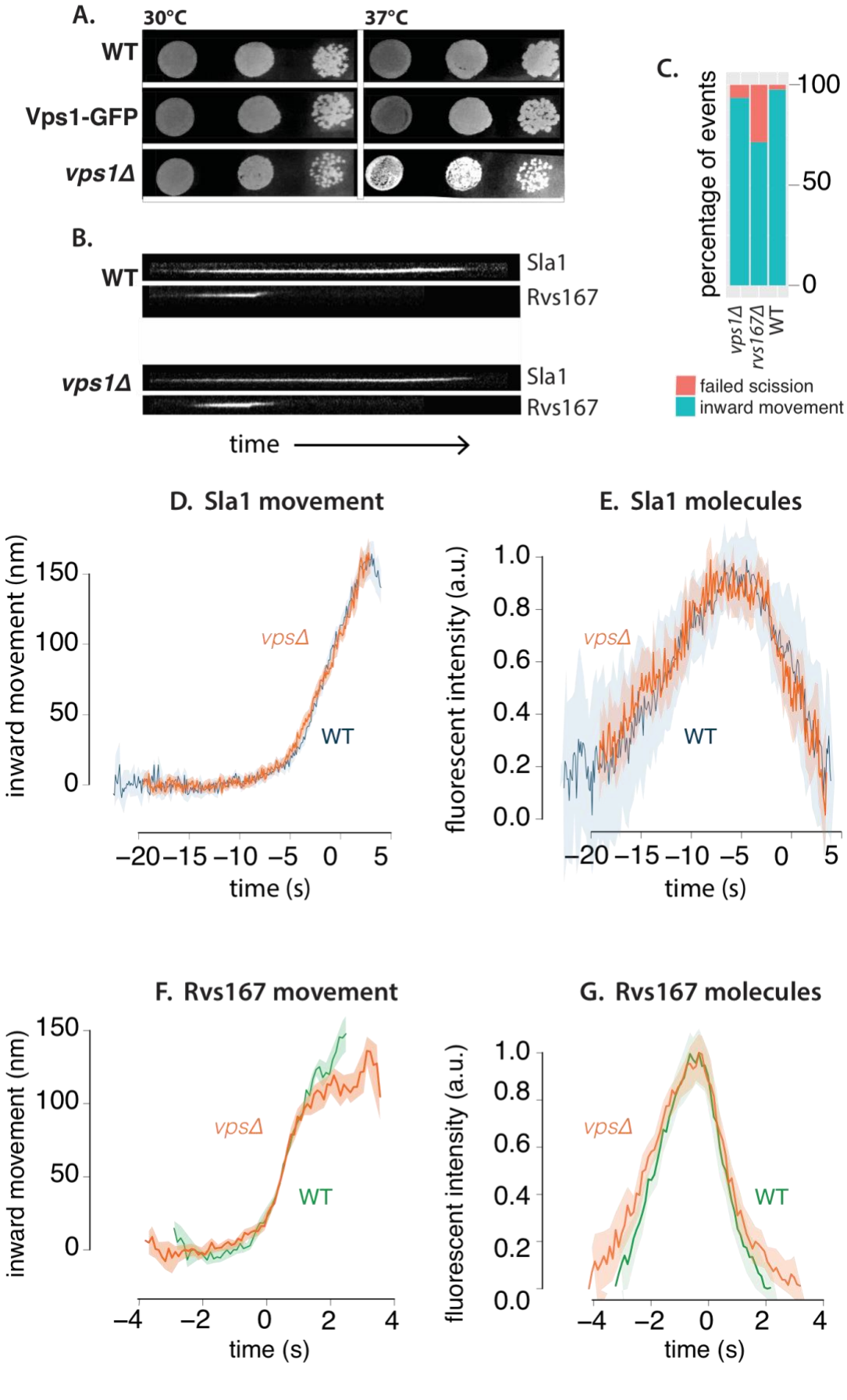

Fig.2.5 A: Dot spots of yeast cells in WT, Vps1-GFP, and vpsdel cell at 30C and 37C. vpsdel cells show a slight growth defect at 37C that is not seen in Vps1-GFP strain.
B: Kymographs of Sla1-GFP and Rvs167-GFP in WT and vpsdel cells show similar assembly/ disassembly. Exposure 80ms.
C: Failure rate of membrane scission, measured by quantifying number of retractions of Sla1 after membrane begins to move inwards, or by total lack of movement.
D, E: Averaged centroid movement and normalized fluorescent intensity of Sla1-GFP in WT and vpsdel strains. Time =0 (s) for WT Sla1 centroid is aligned to Abp1 fluorescent intensity maximum. Sla1 for vpsdel is shifted in time to move inwards at the same time as WT.
F, G: Averaged centroid movement and normalized fluorescent intensity of Rvs167-GFP in WT and vpsdel strains. Time =0 (s) for WT Rvs167 centroid is aligned to Abp1 fluorescent intensity maximum. Rvs167 for vpsdel is shifted in time so that fluorescent intensity maxima is at time=0 (s).

Can lipid hydrolysis cause scission?

Another hypothesis has proposed that regulated lipid hydrolysis can cause vesicle scission[19]. Phosphatidylinositols (PIs) and their derivatives play important roles in many cellular processes including membrane trafficking and cell signalling. Conversion between lipid types is driven by kinases, lipases, and phosphatases and controlled throughout the membrane trafficking pathway.

Phosphatidylinositol(4,5)-biphosphate (PI(4,5)P2) is an important lipid type found at the cell surface, and is enriched and depleted from endocytic sites at the plasma membrane in concert with the assembly and disassembly of the endocytic machinery. Synaptojanins form a subset of inositol polyphosphate 5-phosphatases that hydrolyze PI(4,5)P2 to PI(4)P by removing the phosphate at the 5' position of the inositol ring, and play a role in CME and intracellular signalling, as well as in modulating the actin cytoskeleton[19]. Synaptojanins localize to endocytic sites, and in mammalian cells, disruption of Synaptojanin genes results in cellular accumulation of PI(4,5)P2 and coated vesicles at the plasma membrane, suggesting a role for lipid hydrolysis in releasing coat proteins from nascent vesicles. Synaptojanins contain an N-terminal homology domain with the cytoplasmic domain of the yeast SAC1 gene that is implicated in lipid metabolism, actin morphology, and vesicle transport in the secretary pathway[20]. A central catalytic domain is then followed by a proline-rich C-terminal region that is the canonical interaction partner of SH3 domains: they are known to interact with actin binding proteins and BAR domain proteins, potentiating also a role in membrane invagination and scission.

The yeast genome encodes three Synaptojanin-like proteins- Inp51, Inp52 and Inp53- that regulate phospholipid metabolism. Double deletion of Inp51 and Inp52 has been shown to increase the lifetime of endocytic proteins and produce aberrant membrane invaginations that could indicate scission failure and defective endocytosis, although uptake of extracellular membrane appears to proceed in spite of the morphological aberrations[21,22]. Deletion of Inp52 along with Rvs167 is shown to increase membrane retraction rate, supporting a possible role in membrane scission[23]. Loss of inp51 has led to an increase in bulk PIP2 level, although changes in PIP2 levels have not been reported for mutations of inp52, and are not measured locally at the endocytic sites[24,25].

In a model proposed by Liu et al, Synpatojanins and BAR proteins interact to regulate PI(4,5)P2 hydrolysis, which in turn drives membrane scission. Here, Rvs forms a scaffold on the membrane tube, and protects the underlying PIP2 from hydrolysis. Synaptojanin arrives

at inavaginated membranes, and hydrolyses unprotected PIP2. This generates a boundary between BAR-protected PIP2 at the tube and PIP at the bud tip. The lipid boundary produces a line tension at the interphase that would generate enough force to pinch off a vesicle.

R2.2 Deletion of yeast synaptojanin does not significantly affect coat and Rvs movement

I tested the model proposing lipid hydrolysis as a scission effector by studying the effect of synaptojanin deletion on Sla1 and Rvs167. All analysis discussed below refers to yeast cells imaged at the equatorial plane, expressing GFP and m-Cherry tagged proteins. In all cases, dense clusters of tagged protein at the bud neck are not considered.
First, of the three yeast Synaptojanins, only Inp52-GFP localizes to cortical patches. Dual-color imaging and time alignment with Abp1 as described in Picco et al., shows that Inp52 localizes to endocytic sites at the late stage of scission, along with Rvs. The centroid of Inp52-GFP can be localized to the tip of the invaginated tube, consistent with the Liu theory of membrane scission: spatial and temporal localization is consistent with influence on scission. Inp51-GFP exhibits a diffuse cytoplasmic signal, while Inp53 localizes to patches within the cytoplasm, likely to the trans-golgi network, as has been noted in other work.

Deletion of Inp52 does not affect the speed of membrane invagination, as reported by the movement of the Sla1 centroid. Sla1-GFP patches are assembled and disassembled, as are Rvs167-GFP patches. All Sla1-GFP patches in the movies analysed (n=13 cells) move inwards. 72.9% of Rvs167-GFP patches move inwards into the cytoplasm (n=4 cells, 37patches). Remaining patches are disassembled without apparent inward movement. Vesicle scission appears to occur similar to wild-type, since the Rvs167 centroid moves inwards to approximately the same distance into the cytoplasm, indicating that the base of the vesicles are likely at the same position as in wild-type. Both Sla1 and Rvs167 centroids however, persist post-scission (arrowheads in figure) instead of disassembling immediately like in the WT. Since majority of the patches move inwards, and the increase in the lifetime of Rvs is post-scission, I find that the data is consistent with a role for Inp52 in vesicle uncoating, rather than a primary role in membrane scission, with the aberrations in plasma membrane morphology consequent of failure to recycle components, rather than scission.

Deletion of Inp51 does not affect Rvs167 or Sla1 centroid movement. All Sla1-GFP patches move inward (n=19 cells). 93% of Rvs167-GFP patches move inward (n=3 cells, 44 patches), similar to WT. Assembly of Rvs167 in the Inp51_del is slowed, the implication of this delay is not thus far clear.

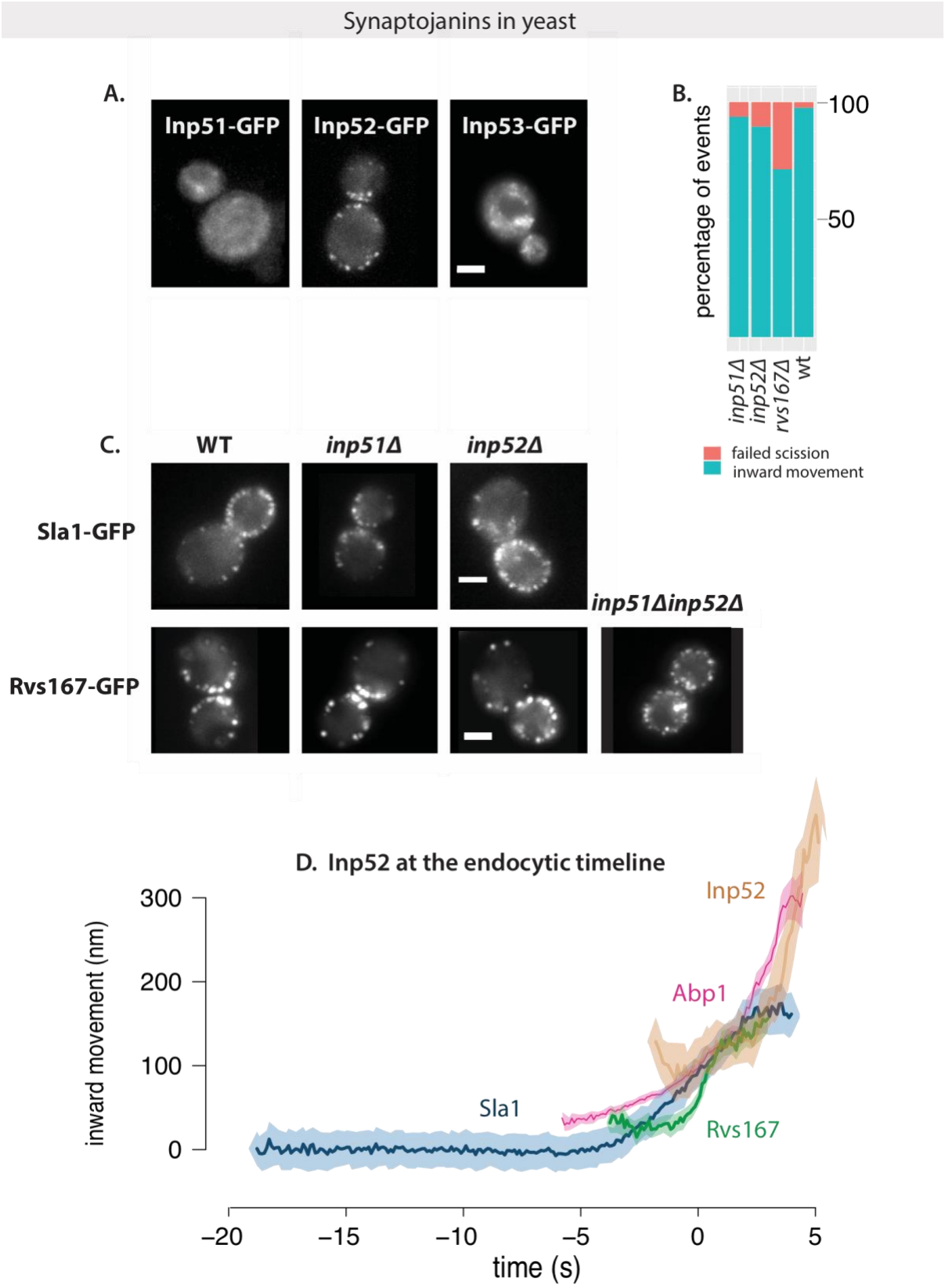

Fig.2.6 A: Localization of GFP-tagged yeast Synaptojanins Inp51, Inp52, and Inp53. Exposure rate 80ms
B: Failure rate of membrane scission, measured by quantifying number of retractions of Sla1 after membrane begins to move inwards, or by total lack of movement in WT, rvsdel, inp51del and inp52del strains.
C: Sla1-GFP in WT, inp51del and inp52del strains show similar plasma membrane localization. Rvs167-GFP in WT, inp51del, inp52del and inp51delinp52del strains. Rvs in single deletion strains show localizations similar to WT, but double deletion strains consists of large patches

of Rvs167 at the plasma membrane, as well as localized within the cytoplasm.
D: Inp52-GFP in endocytic timeline in WT cells. Time=0 (s) corresponds to the fluorescent intensity maxima of the Abp1-mCherry in simultaneous dual-color imaging Sla1-GFP, Rvs167-GFP, and Inp52-GFP with Abp1-mCherry.

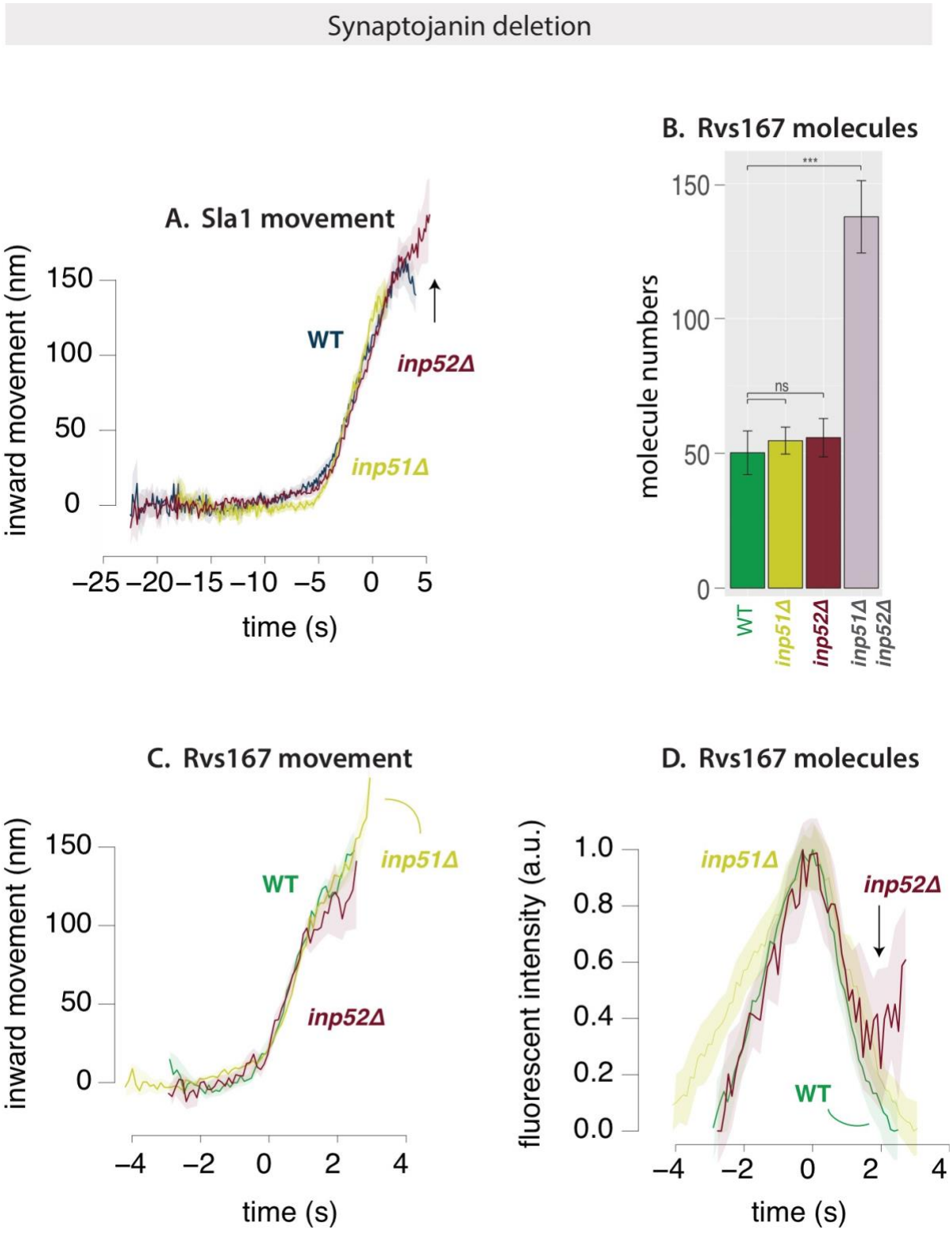

Fig.2.7 A: Averaged centroid movement of Sla1-GFP in WT, inp51del and inp53del strains. Time=0 (s) for WT strains corresponds to fluorescent intensity maxima of Abp1-mCherry in dual-color imaging of cells expressing Sla1-GFP Abp1-mCherry. Sla1 centroids for inp51del and inp52del have been shifted in time to move inwards at the same time as the WT strain.
B: Median molecule numbers of Rvs167-GFP in WT, inp51del and inp52del strains.
C: Averaged centroid movement of Rvs167-GFP in WT, inp51del and inp52del strains. Time=0 (s) for WT Rvs167-GFP corresponds to

fluorescent intensity maxima of Abp1-mCherry in dual-color imaging of cells expressing Rvs167-GFP, Abp1-mCherry. Rvs167-GFP for inp51del, inp52del strains have been shifted so that Time=0 (s) corresponds to time of maximum fluorescent intensity of corresponding Rvs167-GFP centroids.

WT levels of Rvs167 are recruited in both Inp51_del and Inp52_del cases. In Inp5152_double deletion however, nearly three times as much Rvs is recruited to sites. Rvs167-GFP patches in these cells assemble and disassemble, although many large clusters are present on the plasma membrane, and the regular inward jump of Rvs in WT is not seen. Some cytoplasmic patches are also seen, consistent with earlier observations of Sla1 patches within the cytoplasm[26]. These patches likely mark aberrant membrane invaginations continuous with the plasma membrane that are able to assemble and disassemble endocytic patches. Sla1 patches, are however, motile in the double deletion cells, suggesting that membrane scission still occurs in these cells[26]. Analysis of the double deletion phenotype is compounded by the accumulation of Rvs: if vesicles are not stripped of Rvs and other endocytic proteins, we are unable to distinguish between membrane tubes and vesicles that remain in the vicinity of newly forming membrane tubes. Further, this failure to recycle endocytic components affects recruitment of these proteins to new endocytic sites and we cannot, with this data, distinguish between scission failure and failure to recruit protein. That the double deletion is worse than the single deletion suggests overlapping function, as also suggested earlier[27]: combining mutations of inp52 and inp51 results in huge cellular morphological defects, and are purported to arise from their involvement in two different pathways.

Can protein friction cause membrane scission ?

Recent *in-vitro* experiments have proposed protein friction as a mechanism by which membrane scission could occur via BAR domain proteins in the absence of dynamin[28]. In this model, a BAR domain scaffold on a membrane tube forms a frictional barrier to lipid diffusion. Forces that pull on the membrane, such as those exerted by motor proteins like myosins or actin polymerization, increase the frictional force exerted by the scaffold on the underlying membrane tube, increasing membrane tension in the bare region of the tube caused by membrane thinning from the lack of lipid influx to this region. Eventually, membrane pores form in this portion of the tube, leading to breaking the tube, and formation of a vesicle. Such a friction-dependent membrane scission model would predict that if more BAR proteins are added to the membrane, frictional force would increase, and scission should occur faster, that is, at shorter invagination lengths than with fewer BAR proteins. Essentially, this model requires a friction-inducing BAR scaffold, and a force that pulls the membrane under it. In yeast CME, this combination is provided by the Rvs complex and polymerization of the actin network respectively.

R2.3 Membrane scission does not occur at shorter tube lengths when recruitment of Rvs is increased

To test whether protein friction could influence membrane scission in yeast, I duplicated the Rvs167 and Rvs161 genes as described in Huber et al. Gene duplication is performed in haploid cells to produce strains that have one (WT Rvs) and two copies of both Rvs161 and Rvs167 (2x Rvs-h). These haploid strains are then mated to generate diploid strains that have four copies of the Rvs167 and Rvs161 genes (4x Rvs), two copies (2x Rvs). Strains containing

1x copy of each Rvs is generated by crossing rvs167_del strain with an rvs161_del strain (1x Rvs).

Rvs copy number titration in haploids

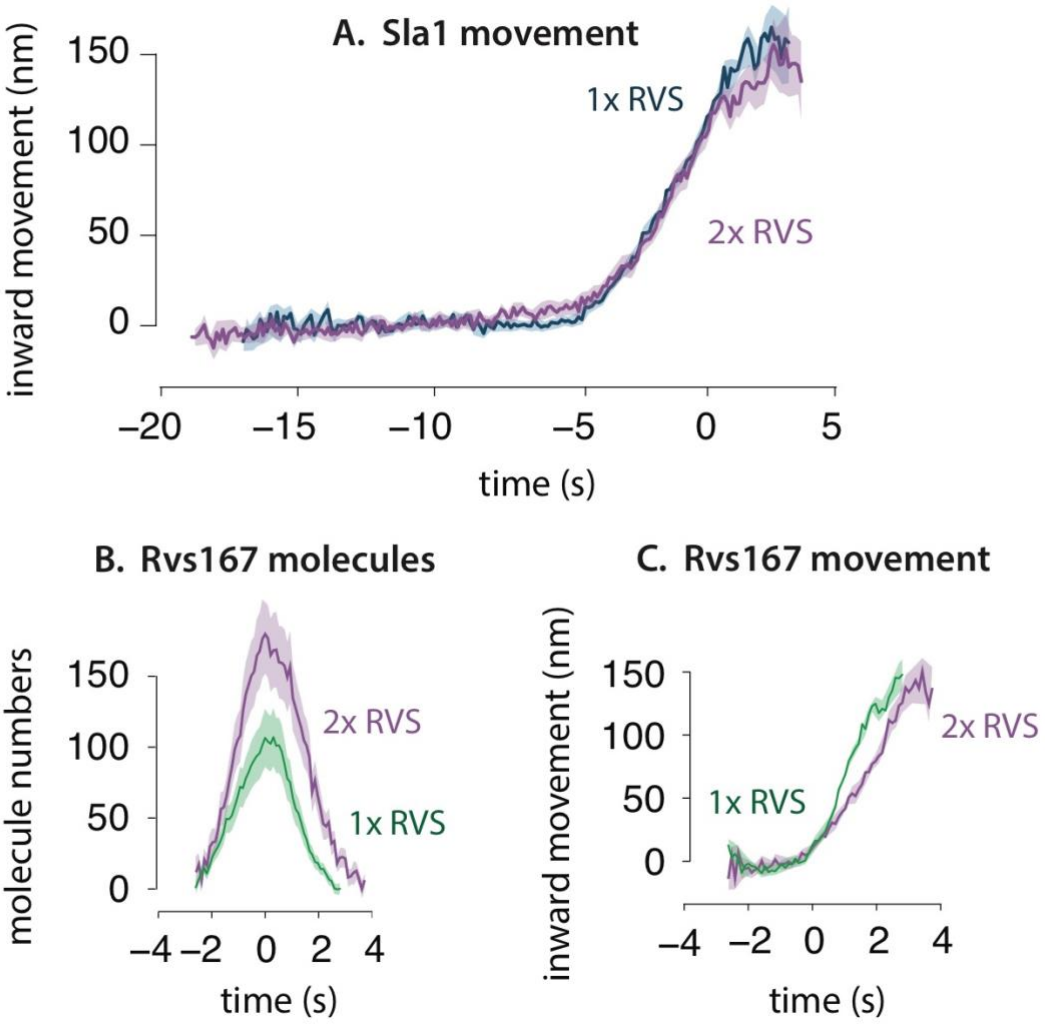

By scaling the number of Rvs167 proteins at endocytic patches in the haploid strains against Nuf2, as described in Picco et al.[2], I found the median and maximum number of Rvs molecules recruited to endocytic sites. The maximum number of Rvs molecules recruited in the 2x Rvs-h strain is 180, compared to 114 (see TABLEx) for WT: 1.6x more Rvs is recruited to endocytic sites in the gene duplicated strain. The averaged trajectory of Sla1-GFP, however does not change between the WT and 2x Rvs-h: like in the WT, Sla1 moves in to about 130nm. After scission, the centroid appears to be slightly lower in the 2x Rvs-h case than in WT, but the GFP signal in this time window after scission is from a diffusing vesicle and a disassembling Sla1 patch, and so is too noisy to analyse.

The dynamics of Rvs, however is quite different: In Fig.x , the centroid movement of both WT and 2x Rvs-h are aligned so that time=0 corresponds to the maxima of the fluorescent intensity, which corresponds to scission time. Molecule numbers of 2x Rvs-h increases at a faster rate than WT, and disassembly is slowed by ~1 second. In the corresponding Rvs centroid movement traces, instead of the sharp jump seen in WT, there is a delay in

movement into the cytoplasm.

Rvs titration in diploids

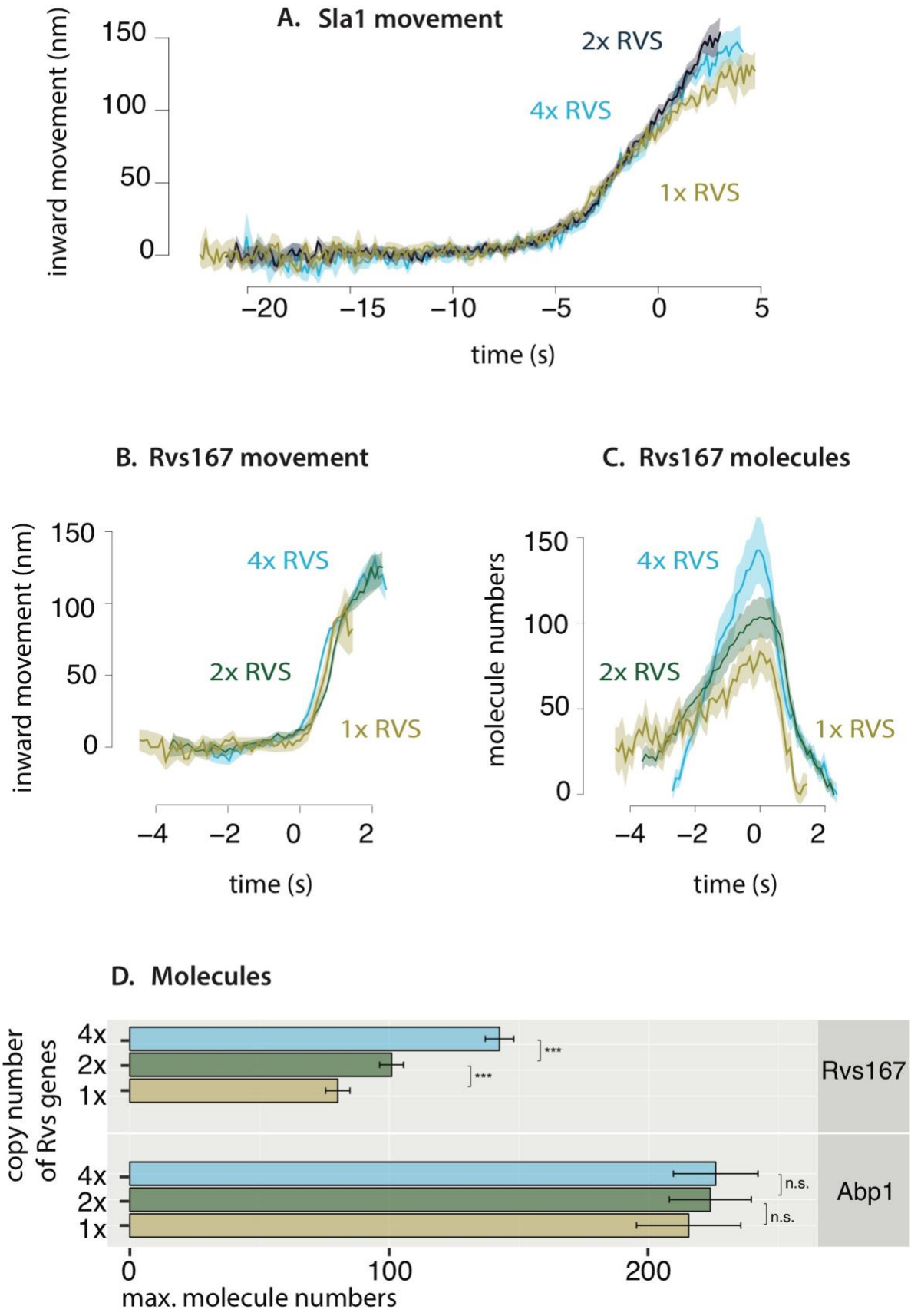

Fig.2.7 A: Averaged centroid movement of Sla1-GFP in diploid strains consisting of 1, 2, and 4 copies of the Rvs161 and Rvs167 genes. Sla1-GFP for 2x and 4x copies of Rvs are aligned so that Time=0 (s) corresponds to fluorescent intensity maxima of Abp1-mCherry in corresponding dual-color imaging. Sla1-GFP for 1x strain was shifted to move inwards at the same time as the other two.
B:

In diploid cells, recruitment of Rvs is similarly measured. Recruitment of Rvs is not directly proportionate to gene copy number: maximum number of Rvs recruited increases from 101 from in the 2x Rvs strain to 143 in the 4x strain (see TABLEX). In the 1x Rvs strain, 80 molecules of Rvs are recruited before scission occurs. In order to determine whether this is a reflection on protein availability or if something else limits recruitment of Rvs, I quantified the cytoplasmic intensity of Rvs167-GFP in the respective strains by first producing maximum intensity projections of time-lapse images of these cells, and measuring the intensity within the cytoplasm (for details see METHODS). As can be seen in TABLE.X, the number of molecules recruited to endocytic sites scales with the amount of protein in the cytoplasm.

Inward movement of the Rvs centroid is similar for the 4x, 2x and 1x Rvs: the jump inwards is about 80nm. In the 1x strain, however, the centroid disappears immediately after scission, suggesting that there is reduced Rvs at the base of the newly formed vesicle compared to the WT. Recruitment dynamics of all three are different: in the 4x Rvs strain, Rvs is recruited at a rate of 57 molecules/second, which is reduced to 27 molec/sec for the 2x and 19.07 molec/sec for the 1x strain.

The Sla1 centroid movement, meanwhile is the same in 4x and 2x Rvs strains. In the 1x Rvs strain, Sla1 movement is slightly shifted, suggesting that vesicle scission occurs at invagination lengths about 10nm shorter than that as WT.

R2.4 Amounts Abp1 are the same, irrespective of Rvs gene copy.

As membrane scission is effectively a result of forces acting on the membrane, I measured the amount of Abp1 arriving at endocytic sites as a proxy for the amount of actin, and therefore, as proxy for the forces generated on the membrane. In diploid cells expressing differing gene copies of Rvs, containing Rvs167-GFP and Abp1-mCherry, I compared, as before, the intensities of patches of Abp1 against Nuf2, except that in this case, Abp1 and Nuf2 are tagged with m-Cherry. Even though the number of Rvs molecules recruited is different in the diploid cells expressing varying numbers of genes for Rvs, and Sla1 movement changes slightly in the 1x BAR case, the same amount of Abp1 is recruited to endocytic sites in all three cases.

R2.5 Coat movement is influenced by recruitment of BAR domain

As observed in the previous section, the coat protein movement is in fact affected by recruitment of the Rvs complex, although adding excess protein does not influence it. In R1.2, it can be seen that adding BAR domain alone also affects coat movement. Here, however,

deletion of the SH3 domain results in decreased recruitment of the Rvs protein to endocytic sites. To see whether this reduced coat movement is a result of a loss of the SH3 domain, or a result of reduced protein recruitment, I duplicated, as described before, the BAR domain in haploid yeast cells, resulting in two copies of the BAR domain (2x BAR), and compared coat and scission dynamics in this strain to that of one copy of BAR (1x BAR), full-length Rvs (1x RVS), duplicated Rvs (2x RVS), and rvs167del.

I first compared the recruitment of Rvs in cells expressing BAR-GFP, 2x BAR-GFP, full-length Rvs-GFP (WT). As shown in Fig.x, 1x BAR is recruited at low copy numbers, at 44% that of the WT. Duplication of the BAR to 2x BAR increases sthe recruitment of 62% that of the WT. Correspondingly, WT Sla1 moves inwards at a rate of about 25nm/s. While duplication of the full-length Rvs genes does not change the rate of inward movement of Sla1, this is reduced to 15.625nm/s in 1x BAR case, and increases from this value to 27.5nm/s in the 2x BAR case. Adding BAR domain increases the speed of inward movement, as well as depth to which Sla1 moves. The exact scission point is difficult to determine with the current data, since the Rvs fluorescent intensity is noisy in the 1x BAR and 2x BAR cases. Sla1 centroid in rvs167 deleted cells shows a movement similar to 1x BAR case, is approximately 34.2 nm/s.

BAR duplication in haploids

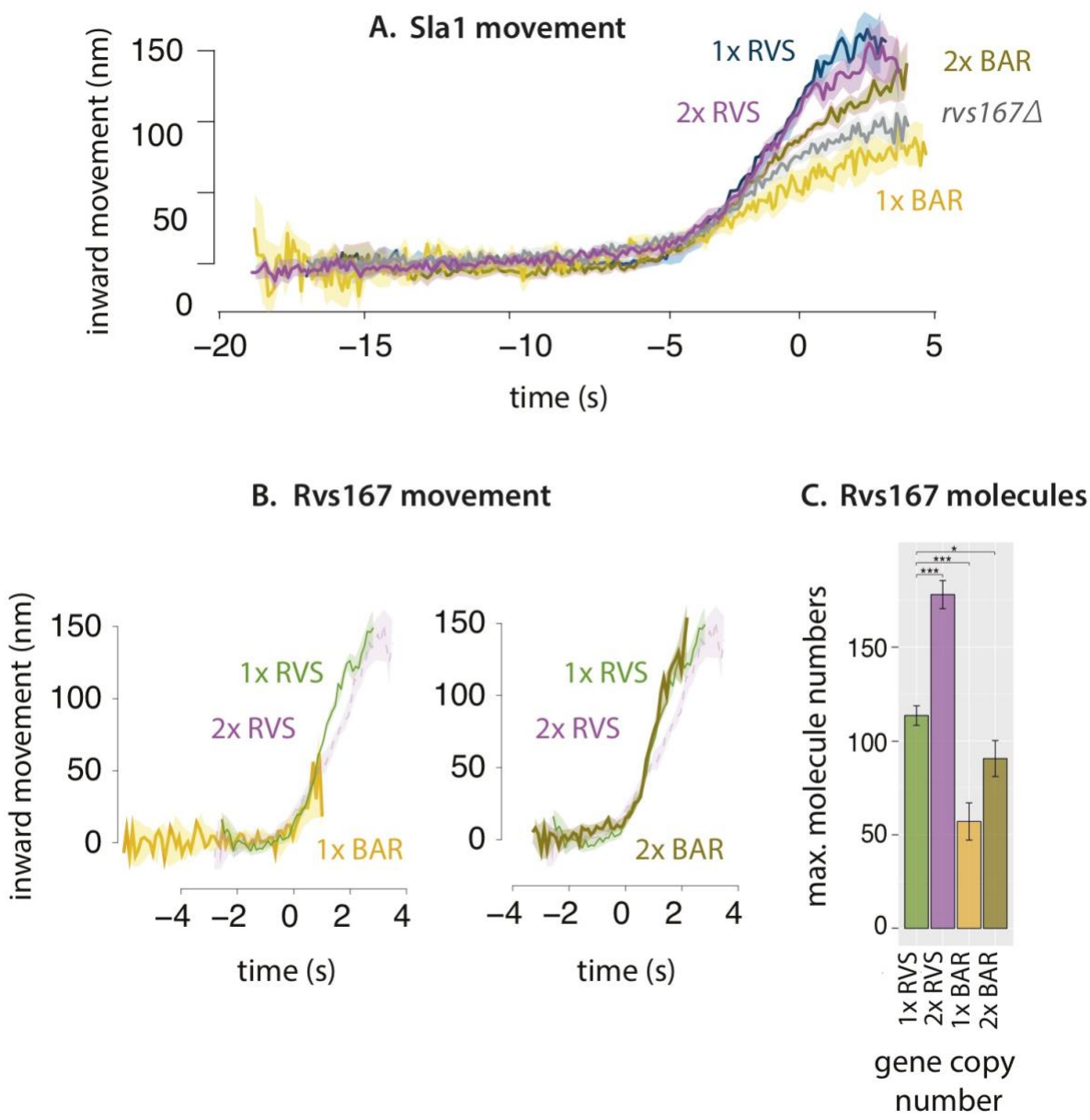

R2.6 Requirement for Rvs is unchanged by membrane tension

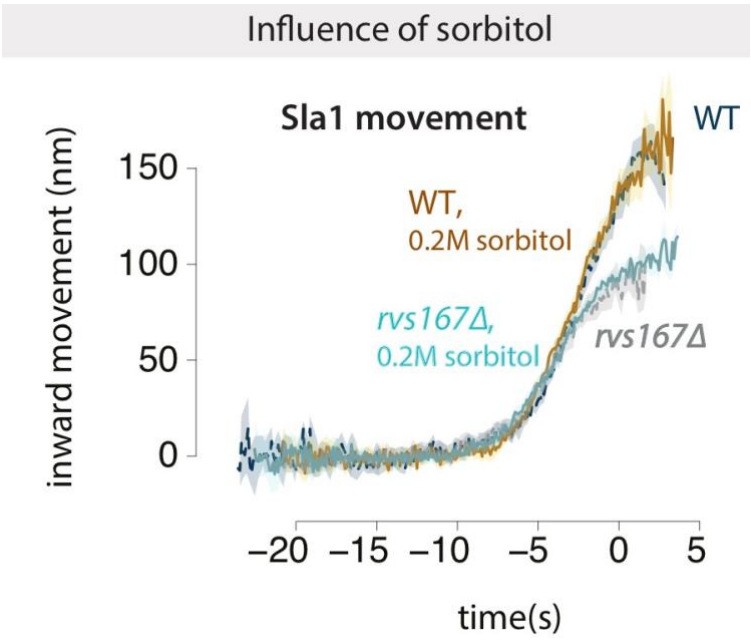
Influence of sorbitol
Sla1 movement
WT
WT,
0.2M sorbitol
rvs167Δ,
0.2M sorbitol
rvs167Δ
inward movement (nm)
150
100
50
0
–20
–15
–10
–5
0
5
time(s)

1. Kaksonen, M., Toret, C. P. & Drubin, D. G. A Modular Design for the Clathrin- and Actin-Mediated Endocytosis Machinery. *Cell* **123,** 305–320 (2005).
2. Picco, A., Mund, M., Ries, J., Nédélec, F. & Kaksonen, M. Visualizing the functional architecture of the endocytic machinery. *Elife* e04535 (2015). doi:10.7554/eLife.04535
3. Kukulski, W., Schorb, M., Kaksonen, M. & Briggs, J. A. G. Plasma Membrane Reshaping during Endocytosis Is Revealed by Time-Resolved Electron Tomography. *Cell* **150,** 508–520 (2012).
4. Stachowiak, J. C., Brodsky, F. M. & Miller, E. A. A cost-benefit analysis of the physical mechanisms of membrane curvature. *Nat. Cell Biol.* **15,** 1019–1027 (2013).
5. Dmitrieff, S. & Nédélec, F. Membrane Mechanics of Endocytosis in Cells with Turgor. *PLoS Comput Biol* **11,** e1004538 (2015).
6. Qualmann, B., Koch, D. & Kessels, M. M. Let's go bananas: revisiting the endocytic BAR code. *EMBO J.* **30,** 3501–3515 (2011).
7. Masuda, M. *et al.* Endophilin BAR domain drives membrane curvature by two newly identified structure-based mechanisms. *EMBO J.* **25,** 2889–97 (2006).
8. Farsad, K. *et al.* Generation of high curvature membranes mediated by direct endophilin bilayer interactions. *J. Cell Biol.* **155,** 193–200 (2001).
9. Peter, B. J. *et al.* BAR Domains as Sensors of Membrane Curvature: The Amphiphysin BAR Structure. *Science (80-.).* **303,** 495–499 (2004).
10. Taylor, M. J., Perrais, D. & Merrifield, C. J. A high precision survey of the molecular dynamics of mammalian clathrin-mediated endocytosis. *PLoS Biol.* **9,** e1000604 (2011).
11. Skruzny, M. *et al.* Molecular basis for coupling the plasma membrane to the actin cytoskeleton during clathrin-mediated endocytosis. *Proc. Natl. Acad. Sci. U. S. A.* **109,** E2533-42 (2012).
12. Kaksonen, M., Sun, Y. & Drubin, D. G. A pathway for association of receptors, adaptors, and actin during endocytic internalization. *Cell* **115,** 475–487 (2003).
13. Verschueren, E. *et al.* Evolution of the SH3 Domain Specificity Landscape in Yeasts. *PLoS One* **10,** (2015).
14. Mayer, B. J. SH3 domains: complexity in moderation. *J. Cell Sci.* **114,** 1253–63 (2001).
15. Sivadon, P., Crouzet, M. & Aigle, M. Functional assessment of the yeast Rvs161 and Rvs167 protein domains. *FEBS Lett.* **417,** 21–7 (1997).
16. Rooij, I. I. S. *et al.* A role for the dynamin-like protein Vps1 during endocytosis in yeast. *J. Cell Sci.* jcs.070508 (2010). doi:10.1242/jcs.070508
17. Nannapaneni, S. *et al.* The yeast dynamin-like protein Vps1:vps1 mutations perturb the internalization and the motility of endocytic vesicles and endosomes via disorganization of the actin cytoskeleton. *Eur. J. Cell Biol.* **89,** 499–508 (2010).
18. Goud Gadila, S. K. *et al.* Yeast dynamin Vps1 associates with clathrin to facilitate vesicular trafficking and controls Golgi homeostasis. *Eur. J. Cell Biol.* **96,** 182–197 (2017).
19. McPherson, P. S. *et al.* A presynaptic inositol-5-phosphatase. *Nature* **379,** 353–357 (1996).
20. Kearns, B. G. *et al.* Essential role for diacylglycerol in protein transport from the yeast Golgi complex. *Nature* **387,** 101–105 (1997).
21. Srinivasan, S. *et al.* Disruption of three phosphatidylinositol-polyphosphate 5-phosphatase genes from Saccharomyces cerevisiae results in pleiotropic abnormalities of vacuole morphology, cell shape, and osmohomeostasis. *Eur. J. Cell Biol.* **74,** 350–60

(1997).
22. Singer-Krüger, B., Nemoto, Y., Daniell, L., Ferro-Novick, S. & De Camilli, P. Synaptojanin family members are implicated in endocytic membrane traffic in yeast. *J. Cell Sci.* 111 (Pt 2, 3347–3356 (1998).
23. Kishimoto, T. *et al.* Determinants of endocytic membrane geometry, stability, and scission. *Proc. Natl. Acad. Sci.* 108, E979–E988 (2011).
24. Stolz, L. E., Huynh, C. V, Thorner, J. & York, J. D. Identification and Characterization of an Essential Family of Inositol Polyphosphate 5-Phosphatases (INP51, INP52 and INP53 Gene Products) in the Yeast Saccharomyces cerevisiae.
25. Stefan, C. J., Audhya, A. & Emr, S. D. The Yeast Synaptojanin-like Proteins Control the Cellular Distribution of Phosphatidylinositol (4,5)-Bisphosphate. *Mol. Biol. Cell* 13, 542–557 (2002).
26. Sun, Y., Carroll, S., Kaksonen, M., Toshima, J. Y. & Drubin, D. G. PtdIns(4,5)P2 turnover is required for multiple stages during clathrin- and actin-dependent endocytic internalization. *J. Cell Biol.* 177, 355–367 (2007).
27. Stolz, L. E., Kuo, W. J., Longchamps, J., Sekhon, M. K. & York, J. D. INP51, a yeast inositol polyphosphate 5-phosphatase required for phosphatidylinositol 4,5-bisphosphate homeostasis and whose absence confers a cold-resistant phenotype. *J. Biol. Chem.* 273, 11852–61 (1998).
28. Simunovic, M. *et al.* Friction Mediates Scission of Tubular Membranes Scaffolded by BAR Proteins. *Cell* 170, 1–13 (2017).

Legends:

inp

{A: Maximum intensity projections of time-lapse images of cells expressing GFP-tagged Synaptojanin-like proteins Inp51, Inp52, and Inp53. Exposure rate 80ms.

B: Failure rate of membrane scission, measured by quantifying number of retractions of Sla1 after membrane begins to move inwards, or by total lack of movement in WT, rvsdel, inp51del and inp52del strains.

C: Sla1-GFP in WT, inp51del and inp52del strains show similar plasma membrane localization. Rvs167-GFP in WT, inp51del, inp52del and inp51delinp52del strains. Rvs in single deletion strains show localizations similar to WT, but double deletion strains consists of large patches of Rvs167 at the plasma membrane, as well as localized within the cytoplasm.

D: Inp52-GFP in endocytic timeline in WT cells. Time=0 (s) corresponds to the fluorescent intensity maxima of the Abp1-mCherry in simultaneous dual-color imaging Sla1-GFP, Rvs167-GFP, and Inp52-GFP with Abp1-mCherry.

All scale bars =2um.

Inp_del

{A: Movement of Sla1 in WT, Inp51del and Inp52del strains.

B: Median number of Rvs167 molecules recruited to endocytic sites in WT, \textit{inp52Δ }, \textit{inp52Δ } and

\textit{inp51Δinp52Δ } cells. P-values from two-sided z test, * = p $\leq$ 0.05 , ** = p$\leq$ 0.01, *** = p $\leq$ 0.001.

C: Movement of Rvs167 in WT, \textit{inp51Δ } and \textit{inp52Δ } strains.

D: Normalized fluorescent intensity of averaged Rvs167 patches in WT, \textit{inp51Δ }, \textit{inp52Δ } cells.

Rvs haploid

\begin{figure}[h]
\centering

\includegraphics[width=15cm,height=15cm,keepaspectratio]{figures/results_final/rvs_haploid}
\caption[Overexpression of the Rvs complex in haploid cells]
{A. Movement of Sla1 in WT (1x RVS) and gene-duplicated Rvs (2x RVS) cells. 1x RVS Sla1 is aligned so that time=0 (s) is scission time. 2x RVS Sla1 is shifted to move inwards at the same time.

B. Recruitment of Rvs167 to sites in WT (1x Rvs) and gene-duplicated Rvs (2x RVS) cells.1x RVS is aligned so that time = 0 (s) is scission time. 2x RVS Sla1 is shifted to move inwards at the same time.

C. Movement of Rvs167-GFP in WT (1x RVS) and gene-duplicated Rvs (2x RVS) cells. 1x RVS Rvs167 is aligned so that time=0 (s) is scission time. 2x RVS Rvs167 is shifted to move inwards at the same time.
\label{fig_rvshaploid}}
\end{figure}

Rvs diploid

\begin{figure}[h]
\centering

\includegraphics[width=21cm,height=21cm,keepaspectratio]{figures/results_final/protein_friction2}
\caption[Dynamics of endocytosis in diploid strains with gene duplicated Rvs]
{A. Movement of Sla1 in WT (1x RVS) and gene-duplicated Rvs (2x RVS) cells. 1x RVS Sla1 is aligned so that time=0 (s) is scission time. 2x RVS Sla1 is shifted to move inwards at the same time.

B. Recruitment of Rvs167 to sites in WT (1x Rvs) and gene-duplicated Rvs (2x RVS) cells.1x RVS is aligned so that time = 0 (s) is scission time. 2x RVS Sla1 is shifted to move inwards at the same time.

C. Movement of Rvs167-GFP in WT (1x RVS) and gene-duplicated Rvs (2x RVS) cells. 1x RVS Rvs167 is aligned so that time=0 (s) is scission time. 2x RVS Rvs167 is shifted to move inwards at the same time.

\label{fig_rvsdiploid}}

\end{figure}